Journal of Power Sources 196 (2011) 3678–3682

Contents lists available at ScienceDirect

Journal of Power Sources

journal homepage: www.elsevier.com/locate/jpowsour

Short communication

# Pore-size effect on photovoltaic performance of dye-sensitized solar cells composed of mesoporous *anatase*-titania

Tae Kwan Yun[a], Sung Soo Park[b], Duckhyun Kim[b], Yong-Kyung Hwang[c], Seong Huh[c], Jae Young Bae[a,*], Yong Sun Won[b,**]

[a] Department of Chemistry, Keimyung University, Daegu 704-701, Republic of Korea
[b] Corporate R&D Center, Samsung SDI Co. Ltd., Gongse-dong, Yongin, Gyunggi 446-577, Republic of Korea
[c] Department of Chemistry and Protein Research Center for Bio-Industry, Hankuk University of Foreign Studies, Yongin 449-791, Republic of Korea

ARTICLE INFO

*Article history:*
Received 28 September 2010
Received in revised form
23 November 2010
Accepted 25 November 2010
Available online 21 December 2010

*Keywords:*
Dye-sensitized solar cell (DSSC)
Mesoporous
Titania

ABSTRACT

The effect of the pore size of mesoporous *anatase*-$TiO_2$ on the photovoltaic performance of dye-sensitized solar cells (DSSCs) is investigated. The mesoporous $TiO_2$ particles are synthesized by two different methods using a soft template of tri-block copolymer and a hard template of mesoporous ZnO/$Zn(OH)_2$-composite. These methods produce the same high surface area ($S_{BET} \sim 210\ m^2\ g^{-1}$) but different pore sizes of 6.8 and 3.0 nm, respectively. With the mesoporous $TiO_2$ having larger pores, the photo-conversion efficiency ($\eta$) is increased significantly to 6.71%, compared with 5.62% that is typically achieved using P25 $TiO_2$ nanopowders. By comparison, only half the performance (3.05%) has been observed with mesoporous $TiO_2$ that has small pores. Mesoporous $TiO_2$ with suitable pore sizes (~6.8 nm) makes the most of its high surface area and thereby allows a high uptake of dye to enhance the current density. In contrast, the low efficiency of mesoporous $TiO_2$ with small pores is attributed to the low uptake of dye due to the smaller pore size (~3.0 nm), which blocks the diffusion and adsorption of dye molecules through the pores.



## 1. Introduction

Over the past decades, there has been increasing interest in the application of $TiO_2$ with high surface area to catalysts, photocatalysts, gas sensors, and self-cleaning panels [1–6]. In particular, dye-sensitized solar cells (DSSCs) have recently become an important application of $TiO_2$ [7–11]. In such devices, the porous $TiO_2$ photoelectrode plays the essential role of transferring electrons from the dye molecules to the transparent conductive oxide (TCO) anode, allowing electrolytes to diffuse inside and supply electrons to the dye molecules adsorbed on the $TiO_2$ surface. A paste composed of *anatase*-$TiO_2$ nanoparticles (12–20 nm) is typically used for fabrication of the photoelectrode on TCO by screen printing and annealing [12]. It has often called a mesoporous $TiO_2$ film due to the presence of mesopores, which are voids formed among the necked $TiO_2$ nanoparticles during the annealing process [13]. In addition to these intercrystalline aggregates, there have been several attempts to synthesize mesoporous $TiO_2$ (denoted as MP-$TiO_2$, hereafter) particles with internally integrated pores by using templates [10,11,14,15]. These mesoporous $TiO_2$ particles are expected to have a more regular and continuous framework, thereby allowing better electron and electrolyte diffusion in the DSSCs applications and even higher surface area for an enhanced uptake of dye. Nevertheless, the influence of pore size on the performance of DSSCs composed of MP-$TiO_2$ has rarely been investigated. Most recently, Hwang et al. [16] have reported that the adsorption properties of N719 dye molecules and the photoconversion efficiency of DSSCs are dependent on the pore size. The authors synthesized MP-$TiO_2$ using silica templates to generate different pore sizes, but these samples ultimately had different surface areas [16].

In the present work, two different MP-$TiO_2$ samples are synthesized to investigate the effect of the pore size on the photovoltaic performance of DSSCs. The first sample (A) is produced by using a soft tri-block copolymer template and the second (B) by using a hard mesoporous ZnO/$Zn(OH)_2$-composite template. These are engineered to be of the same surface area while having different pore sizes. The photoconversion efficiencies of DSSCs based on MP-$TiO_2$ samples (A) and (B) are measured and compared against standard Degussa P25 $TiO_2$ nanopowders. Electrical impedance spectroscopy (EIS) is used to explain differences in the performance of the MP-$TiO_2$-based DSSCs with respect to pore size.

* Corresponding author. Tel.: +82 53 580 5186; fax: +82 53 580 6795.
** Corresponding author. Tel.: +82 31 288 4898; fax.: +82 31 288 4447.
*E-mail addresses:* jybae@kmu.edu (J.Y. Bae), yongsun.won@samsung.com (Y.S. Won).

0378-7753/$ – see front matter © 2010 Elsevier B.V. All rights reserved.
doi:10.1016/j.jpowsour.2010.11.162

## 2. Experimental details

### 2.1. Synthesis of mesoporous titania and characterization

All the details of the synthesis a characterization of MP-$TiO_2$ (B) using the hard template of $ZnO/Zn(OH)_2$ composite have been reported elsewhere [15]. Crystalline mesoporous $ZnO/Zn(OH)_2$ nanocomposite spheres were prepared by a facile one-step synthetic route, and subsequently employed as a hard template for the sol–gel preparation of amorphous mesoporous $TiO_2$ with $Ti(iPrO)_4$ as a precursor. The hydrolytically unstable nature of the $ZnO/Zn(OH)_2$ spheres made the etching process by HCl solution both simple and efficient. The amorphous $TiO_2$ was then crystallized above 350 °C to produce *anatase*-MP-$TiO_2$ (B).

Details of the synthesis and characterization of MP-$TiO_2$ (A) using the soft template of tri-block copolymer have been presented elsewhere [17,18]. MP-$TiO_2$ (A) with an *anatase* framework was synthesized by assembling nanocrystalline particles. A typical synthesis process was as follows. The $TiCl_4$ was dissolved in distilled water (0.2 mol $L^{-1}$) in an ice-water bath. This aqueous solution was then added to $(NH_4)_2SO_4$ in a temperature-controlled bath with continuous stirring at 90 °C for 24 h for preparation of the *anatase* phase. The resulting mixture was cooled to room temperature, and then a P-123 ($EO_{20}PO_{70}EO_{20}$) solution was added while stirring. After stirring for 2 h, the pH value of the reaction was controlled at approximately 4.0 by adding tetramethylammonium hydroxide (TMAOH). The molar ratio of $TiCl_4$:P–123:$H_2O$ was 1:0.036:370. The final reaction temperature was kept at 50 °C for 48 h. The deposit was washed with distilled water twice in a centrifugal separator, filtrated and then dried at 80 °C overnight and ground into powder. The powder was then calcined at 400 °C for 6 h in an airflow.

High-angle (20–80°) X-ray powder diffraction (XRD) patterns were obtained on a PANalytical diffractometer (X'pert PRO MRD) with CuKα radiation (40 kV and 25 mA). The high-angle XRD scanning rate was $5.6 \times 10^{-4}$ $s^{-1}$. Nitrogen adsorption–desorption data were collected on a Quantachrome QUADRASORB SI analyzer at 77 K. Prior to experiment, the samples were dehydrated at 200 °C under vacuum for 2 h. The specific surface area was determined from the linear portion of the Brunauer–Emmett–Teller (BET) equation ($P/P^0$ = 0.05–0.30). The pore-size distribution was calculated using the Barret–Joyner–Halenda (BJH) model. The morphologies of MP-$TiO_2$ samples were observed on Cu grids supported by holey carbon films using a field emission TEM (a FEI Tecnai G2 F20 S-Twin, 200 kV).

### 2.2. Fabrication of DSSCs and performance measurements

To prepare the working electrodes of DSSCs, the P25, MP-$TiO_2$ (A) and (B) samples were first dispersed into a mixture of ethyl cellulose (EC) binder (EC/$TiO_2$ = 30 wt.%) and terpineol solvent. Further mixing was followed by using a thinky mixer for 20 min to form a slurry. The resulting $TiO_2$ paste was then coated on FTO glass plates by the doctor-blade method and gradually calcined under an airflow successively at 325 °C for 5 min, at 375 °C for 5 min, at 450 °C for 15 min, and at 500 °C for 30 min. After being cooled to 100 °C, the $TiO_2$ electrodes were immersed for surface treatment in the $TiCl_4$ aqueous solution (40 mM) at 50 °C for 20 min and subsequently in the dye solution at room temperature for 24 h. The dye-adsorbed photoelectrode and Pt counter electrode were assembled into a sealed sandwich-type cell. A drop of electrolyte solution was then placed on a drilled hole in the counter electrode of the assembled cell and was driven into the cell by means of vacuum backfilling. The hole was sealed using an additional cover glass. Anhydrous ethanol containing N719 dye (Ru[LL′-(NCS)2], L = 2,2′-bipyridyl-4,4′-dicarboxylic acid, L′ = 2,2′-bipyridyl-4,4′-ditetrabutylammonium carboxylate, 0.3 mM) was used for the dye adsorption, and the electrolyte was composed of 0.62 M 3-butyl-1-methyl imidazolium iodide, 0.07 M iodine, 0.2 M LiI, 0.5 M tert-butylpyridine, 0.3 M 3-amino-5-methylthio-1,2,4-triazole and 0.13 M 3-amino-1,2,4-triazole in acetonitrile. The active area of the dye-coated $TiO_2$ film was 0.180 $cm^2$.

The *J–V* curves were determined with a potentiostat/galvanostat (263A, EG&G Princeton Applied Research, USA) under an illumination of 10–100 mW $cm^{-2}$ from a 50–500 W Xe lamp (Thermo Oriel Instruments, USA). The a.c. impedance measurements were carried out under one sun illumination and dark conditions using an impedance analyzer (1260A, Solartron, UK). FE-SEM images were obtained with a FEI Sirion.

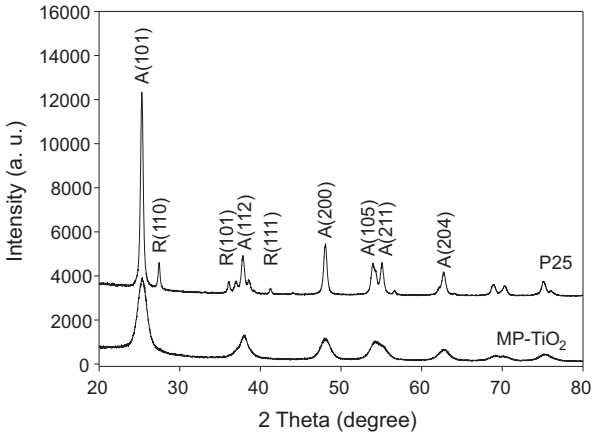


**Fig. 1.** High-angle X-ray diffraction patterns of P25 and MP-$TiO_2$ (A).

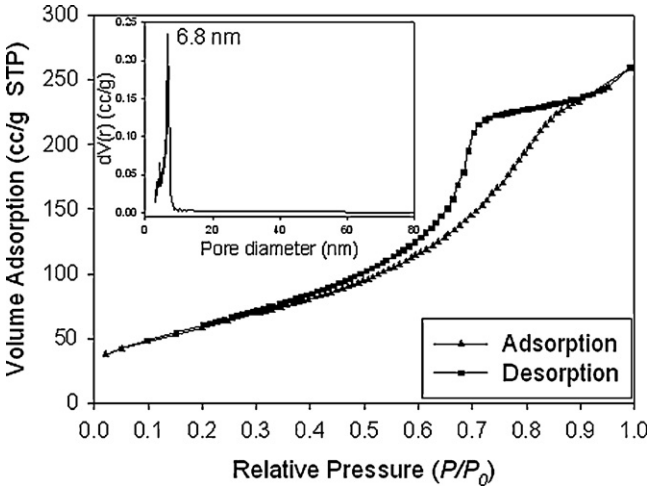


**Fig. 2.** $N_2$ adsorption–desorption isotherms and BJH pore-size distribution plot (insert) of MP-$TiO_2$ (A).

**Table 1**
Pore characteristics of MP-$TiO_2$ using tri-block copolymer (A) and mesoporous $ZnO/Zn(OH)_2$ composite (B) templates. Data for (B) were taken from Ref. [15]. For reference, $S_{BET}$ of P25 was 54 $m^2g^{-1}$.

| Samples | $S_{BET}$ ($m^2g^{-1}$) | Pore size (nm) | Pore volume ($mLg^{-1}$) |
|---|---|---|---|
| MP-$TiO_2$ (A) using soft template | 213 | 6.8 | 0.4 |
| MP-$TiO_2$ (B) using hard template | 202 | 3.0 | 0.26 |

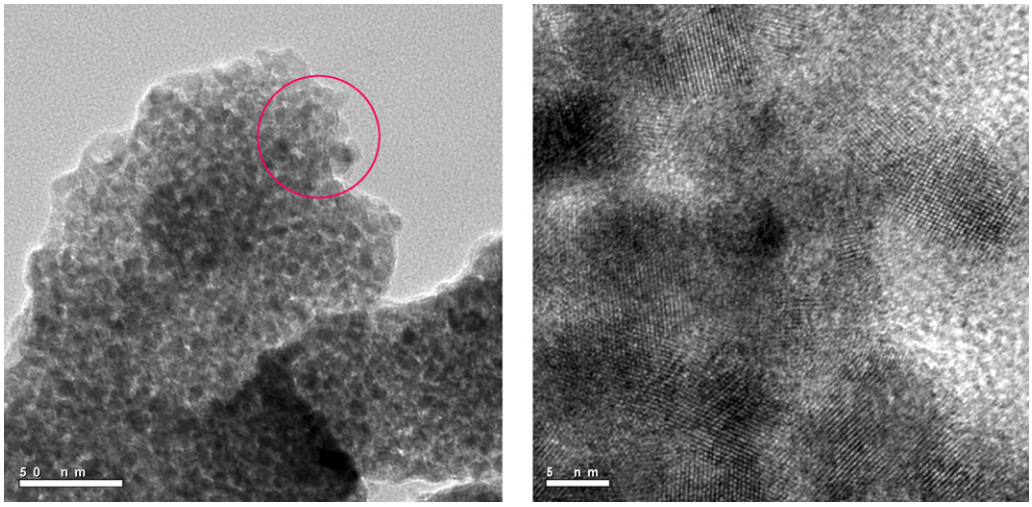


**Fig. 3.** TEM micrographs of MP-$TiO_2$ (A) with different magnifications.

## 3. Results and discussion

### 3.1. Structural properties of mesoporous titania

The structural properties of the synthesized MP-$TiO_2$ were characterized by XRD and $N_2$ adsorption–desorption. The XRD patterns of both MP-$TiO_2$ (A) and (B) are consistent with the structure of *anatase* (JCPDS 21-1272). High-angle XRD patterns of MP-$TiO_2$ (A) and P25 are shown in Fig. 1 for comparison. It is noted that the diffraction pattern of P25 has *anatase* and *rutile* (8:2) structures, which is similar to the reference data of P25 [19]. The XRD pattern of MP-$TiO_2$ (B) is shown in the supplementary material taken from Ref. [15]. The nitrogen adsorption–desorption isotherms and BJH pore-size distribution of MP-$TiO_2$ (A) are presented in Fig. 2, whereas those of MP-$TiO_2$ (B) are presented in the supplementary material taken from Ref. [15]. This type IV isotherm with an H2 hysteresis loop is typical of mesoporous structures [20]. Correspondingly, the high-resolution TEM images in Fig. 3 demonstrate the aggregation of the highly crystalline nature of the nanoparticles to generate porous microstructures for MP-$TiO_2$ (A). Similar images are obtained for MP-$TiO_2$ (B) [15]. The BET specific surface area ($S_{BET}$), pore size, and pore volume of MP-$TiO_2$ samples are summarized in Table 1. They have the same high $S_{BET}$ ($\sim$210 $m^2\,g^{-1}$) but different pore sizes of 6.8 and 3.0 nm for MP-$TiO_2$ (A) and (B),

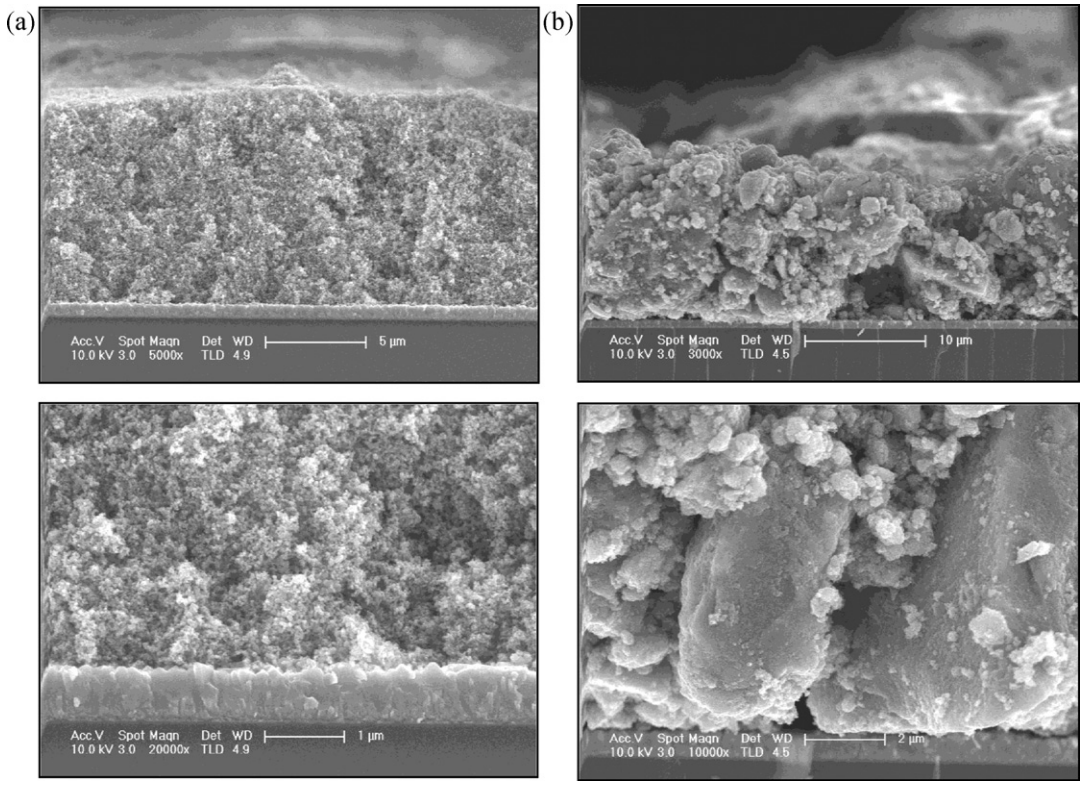


**Fig. 4.** Cross-sectional SEM images for $TiO_2$ electrodes prepared from (a) P25 and (b) MP-$TiO_2$ (A)/(B) at different magnifications. Characterization of samples after $TiCl_4$ post-treatment and dye dipping.

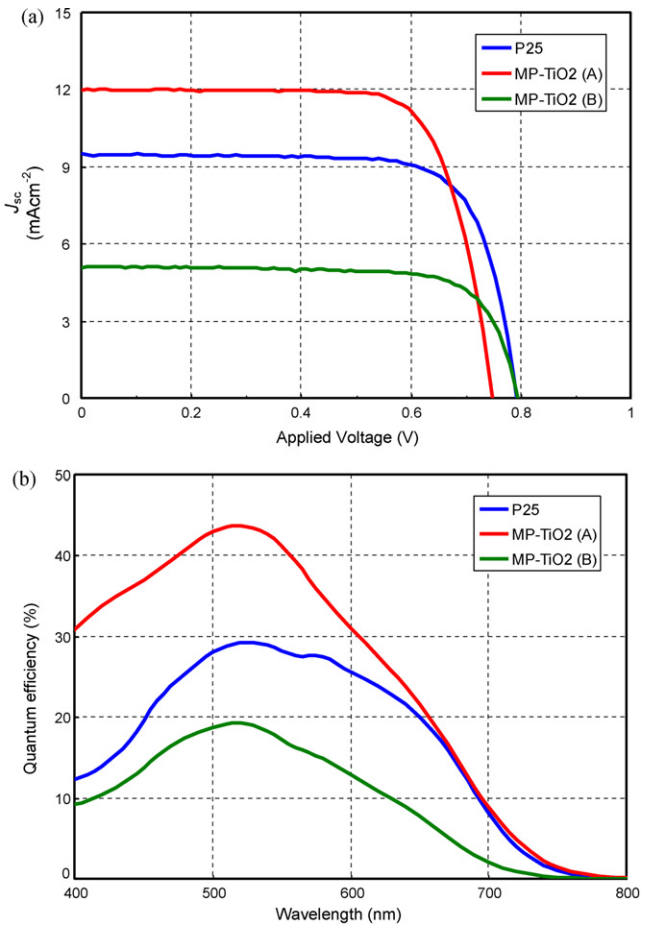


**Fig. 5.** (a) *J–V* curves and (b) IPCE spectra for DSSCs prepared from P25 and MP-$TiO_2$ with $TiCl_4$ post-treatment.

respectively. Therefore, they are an excellent choice for the separate investigation of the pore-size effect on the performance of DSSCs composed of MP-$TiO_2$.

Cross-sectional SEM images of photoelectrodes prepared from P25 and MP-$TiO_2$ are given in Fig. 4. The difference is apparent. Uniform thickness is produced by uniformly close-packed P25 nanoparticles (~20 nm) (Fig. 4a), while a rough layer is formed with loosely stacked MP-$TiO_2$ micron-size particles (Fig. 4b). A regular and continuous mesoporous framework is potentially constructed inside each micron-size particle. The voids between MP-$TiO_2$ micron-size particles possibly become channels for fast-bulk electrolyte diffusion through the layer to wet each micron-size particle fully with bulk electrolyte solution. A much shorter diffusion length of electrolyte results from the surface to the core of each micron-size particle (Fig. 4b), compared with the electrolyte diffusion vertically through the close-packed layer composed of P25 nanoparticles (Fig. 4a). Fast electrolyte diffusion through the layer may, however, pose the counter problem of enhanced electron loss by recombination of electrolytes from bare $TiO_2$ (uncovered by dye molecules) and TCO surfaces.

### 3.2. Pore-size effect on photovoltaic performance of DSSCs

The *J–V* curves and IPCE spectra are shown in Fig. 5, and the photovoltaic properties of DSCs prepared from P25 and MP-$TiO_2$ are summarized in Table 2. The short-circuit current density ($J_{sc}$) increases significantly for MP-$TiO_2$ (A) with large pores, although the open-circuit voltage ($V_{oc}$) slightly decreases, possibly due to its inferior crystallinity. By contrast, only half the performance

**Table 2**
Photovoltaic performances of DSSCs prepared from P25 and MP-$TiO_2$ with $TiCl_4$ post-treatment.

| Samples | $V_{oc}$ (mV) | $J_{sc}$ (mAcm$^{-2}$) | FF (%) | $\eta$ (%) |
|---|---|---|---|---|
| P25 | 794 | 9.50 | 74.5 | 5.62 |
| MP-$TiO_2$ (A) using soft template | 749 | 11.97 | 74.9 | 6.71 |
| MP-$TiO_2$ (B) using hard template | 795 | 5.07 | 75.7 | 3.05 |

$V_{oc}$: open current voltage, $J_{sc}$: short-circuit photocurrent density, FF: fill factor, $\eta$: photo-conversion efficiency.

is obtained with MP-$TiO_2$ (B) with small pores. The IPCE spectra (Fig. 5b) are consistent with the *J–V* curves. The difference in the performance of MP-$TiO_2$-based cells must result from the pore-size difference because they have the same $S_{BET}$ on the same mesoporous framework. It is noted that all the samples were post-treated by a $TiCl_4$ aqueous solution to facilitate the percolation of photo-injected electrons in the photoelectrode with less recombination by enhancing the necking between $TiO_2$ particles [21,22].

The prepared photoelectrodes differed mostly in colour. While MP-$TiO_2$ (A) with large pores has the typical red-wine colour, MP-$TiO_2$ (B) with small pores is pink. This result suggests that the dye may not diffuse through the small pores efficiently; thus, the dye uptake is much lower in MP-$TiO_2$ (B) without occupying all of the $S_{BET}$. The desirable pore size to achieve high uptake of N719 dye has been reported [19] to be approximately twice the molecular size of N719 (1.76 nm) [16]. The Nyquist plots obtained by EIS are

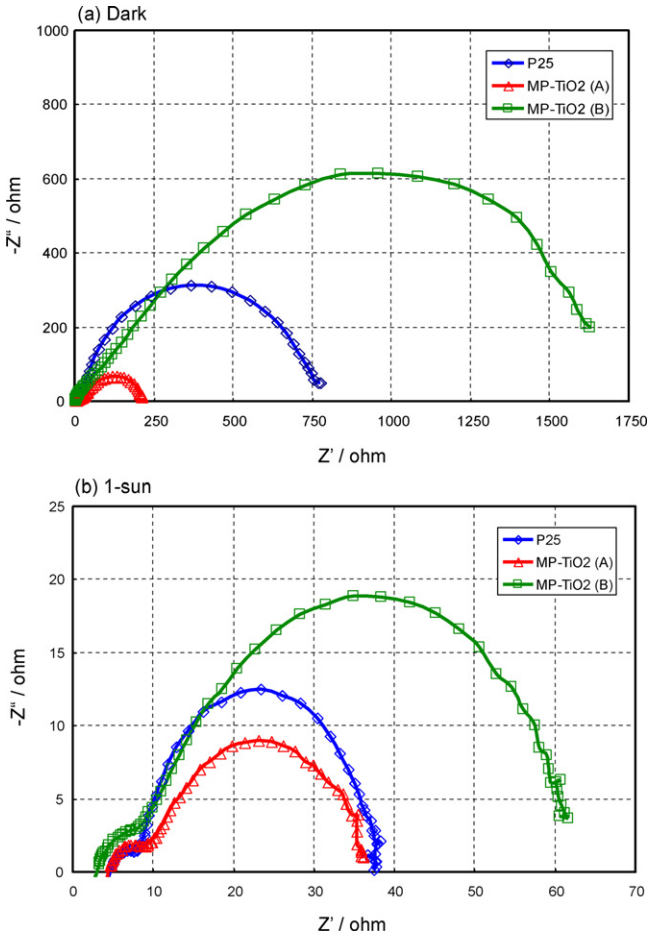


**Fig. 6.** EIS spectra of DSSCs prepared from P25 and MP-$TiO_2$ (a) in dark and (b) under 1-sun illumination. −0.67 V applied in dark, while −0.795, −0.730, and −0.812 V applied for samples prepared from P25, MP-$TiO_2$ (A) and MP-$TiO_2$ (B), respectively, under 1-sun illumination.

shown in Fig. 6. The large arcs at low frequencies comprise electron transfer from $TiO_2$ to the electrolyte and diffusion of $I^{3-}$ ions in the electrolyte [23–26]. Due to the relatively low resistance in the dark (Fig. 6a), the layer prepared from MP-$TiO_2$ (A) has a structure that is inherently susceptible to electron loss by recombination. As shown in Fig. 4, the voids between micron-size particles for MP-$TiO_2$ (A) and (B) become free channels for bulk electrolyte transport deeply through the layer to supply electrolytes more proficiently through the pores. Even with this effect, the small pores in MP-$TiO_2$ (B) are likely to inhibit electrolyte diffusion through the pores, possibly because the dye molecules block the openings of the small pores, and thereby results in the relatively high resistance of MP-$TiO_2$ (B). This is valid for dye diffusion and adsorption through the pores. Therefore, although MP-$TiO_2$ (B) has the advantage of high resistance to electron recombination to electrolytes, the exceedingly low extent of dye uptake cancels it out and reduces the $J_{sc}$ far more, as shown in Fig. 5 and Table 2. The shape of the spectrum of MP-$TiO_2$ (A), however, approaches that of P25 under 1-sun illumination in Fig. 6b. The enhanced resistance in MP-$TiO_2$ (A) indicates that electrons are efficiently withdrawn to the TCO anode with its continuous framework during cell operation, despite its structure being susceptible to electron recombination as suggested by the dark condition (Fig. 6a). In combination with the high uptake of dye using its high $S_{BET}$, the $J_{sc}$ of MP-$TiO_2$ (A) is enhanced significantly compared with P25 (11.97–9.50 mA $cm^{-2}$), as shown in Table 2. The similar small, high-frequency arcs for P25 and MP-$TiO_2$ (Fig. 6b) imply that electron recombination at the of the Pt counter electrode|electrolyte and the TCO|electrolyte [27–30] interfaces is not the most important principle.

## 4. Conclusions

Two *anatase*-MP-$TiO_2$ samples are prepared with two different templates and have the same high $S_{BET}$ but different pore sizes. These are used to investigate the effect of the pore size of MP-$TiO_2$ photoelectrodes on the performance of DSCs. The measured photovoltaic properties suggest that the MP-$TiO_2$ (B) with small pores (~3.0 nm) produces low uptake of the dye and does not utilize its high $S_{BET}$ inside the pores. By contrast, the MP-$TiO_2$ (A) has suitable pore sizes (~6.8 nm) and utilizes its high $S_{BET}$ for high uptake of the dye to enhance the $J_{sc}$ along with efficient electron transport in its continuous framework. The photoconversion efficiency (6.71%) of the MP-$TiO_2$ (A) is a marked improvement on the efficiency of the reference P25 $TiO_2$ nanoparticles (5.62%), while the MP-$TiO_2$ (B) produces only 3.05%. Further experiments on pore-size optimization for maximum DSC performance are still required.

## Appendix A. Supplementary data

Supplementary data associated with this article can be found, in the online version, at doi:10.1016/j.jpowsour.2010.11.162.

## References

[1] W.J. Stark, K. Wegner, S.E. Pratsinis, A.J. Baiker, J. Catal. 197 (2001) 182.
[2] M. Thelakkat, C. Schmitz, H.-W. Schmidt, Adv. Mater. 14 (2002) 577.
[3] D. Morris, R.G. Egdell, J. Mater. Chem. 11 (2001) 3207.
[4] E. Puzenat, P. Pichat, J. Photochem. Photobiol. A 160 (2003) 127.
[5] H.G. Yang, C.H. Sun, S.Z. Qiao, J. Zou, G. Liu, S.C. Smith, H.M. Cheng, G.Q. Lu, Nature 453 (2008) 638.
[6] D. Zhang, G. Li, X. Yang, J.C. Yu, Chem. Commun. (2009) 4381.
[7] M. Wei, Y. Konishi, H. Zhou, M. Yanagida, H. Sugihara, H.J. Arakawa, J. Mater. Chem. 16 (2006) 1287.
[8] Y.J. Kim, M.H. Lee, H.J. Kim, G. Lim, Y.S. Choi, N.-G. Park, K. Kim, W.I. Lee, Adv. Mater. 21 (2009) 3668.
[9] K. Zhu, N.R. Neale, A. Miedaner, A.J. Frank, Nano Lett. 7 (2007) 69.
[10] K. Hou, B. Tian, F. Li, Z. Bian, D. Zhao, C. Huang, J. Mater. Chem. 15 (2005) 2414.
[11] D. Chen, F. Huang, Y.-B. Cheng, R.A. Caruso, Adv. Mater. 21 (2009) 2206.
[12] B. O'Regan, M. Grätzel, Nature 353 (1991) 737.
[13] M. Grätzel, J. Photochem. Photobiol. C 4 (2003) 145.
[14] Y.-Q. Wang, S.-G. Chen, X.-H. Tang, O. Palchik, A. Zaban, Y. Koltypin, A. Gedanken, J. Mater. Chem. 11 (2001) 521.
[15] Y.-K. Hwang, T.-H. Kwon, S.S. Park, Y.-J. Yoon, Y.S. Won, S. Huh, Eur. J. Inorg. Chem. (2010) 4747.
[16] K.-J. Hwang, W.-G. Shim, S.-H. Jung, S.-J. Yoo, J.-W.Lee. Wang, Appl. Surf. Sci. 256 (2010) 5428.
[17] I. Kartini, D. Menzies, D. Blake, J.C.D. da Costa, P. Meredith, J.D. Richesd, G.Q. Lu, J. Mater. Chem. 14 (2004) 2917.
[18] T.A. Ostomel, G.D. Stucky, Chem. Commun. (2004) 1016.
[19] Y. Ma, J. Yao, Chemosphere 38 (1999) 2407.
[20] C.D. Valentin, E. Finazzi, G. Pacchioni, A. Selloni, S. Livraghi, M.C. Paganini, E. Giamello, Chem. Phys. 339 (2007) 44.
[21] S. Ito, T.N. Murakami, P. Comte, P. Liska, C. Grätzel, M.K. Nazeeruddin, M. Grätzel, Thin Solid Films 516 (2008) 4613.
[22] S. Ito, P. Liska, P. Comte, R. Charvet, P. Pechy, U. Bach, L. Schmidt-Mende, S.M. Zakeeruddin, A. Kay, M.K. Nazeeruddin, M. Grätzel, Chem. Commun. (2005) 4351.
[23] Q. Wang, J.–E. Moser, M. Grätzel, J. Phys. Chem. B 109 (2005) 14945.
[24] A. Hauch, A. Georg, Electrochim. Acta 46 (2001) 3457.
[25] J. Qian, P. Liu, Y. Xiao, Y. Jiang, Y. Cao, X. Ai, H. Yang, Adv. Mater. 21 (2009) 3663.
[26] L.-Y. Lin, C.-P. Lee, R. Vittal, K.-C. Ho, J. Power Sources 195 (2010) 4344.
[27] R. Kern, R. Sastrawan, J. Ferber, R. Stangl, J. Luther, J. Electrochim. Acta 47 (2002) 4213.
[28] T. Hoshikawa, M. Yamada, R. Kikuchi, K. Eguchi, J. Electrochem. Soc. 152 (2005) E68.
[29] F. Fabregat-Santiago, J. Bisquert, E. Palomares, L. Otero, D. Kuang, S.M. Zakeeruddin, M. Grätzel, J. Phys. Chem. C 111 (2007) 6550.
[30] F. Fabregat-Santiagoa, J. Bisquert, G. Garcia-Belmonte, G. Boschloo, A. Hagfeldt, Sol. Energy Mater. Sol. Cells 87 (2005) 117.